RC 22519 (W0207-069) July 16, 2002
Physics

IBM Research Report

Sub-Angstrom Resolution Using Aberration Corrected Electron Optics

Philip E. Batson
IBM Research Division
Thomas J. Watson Research Center
P.O. Box 218
Yorktown Heights, NY 10598

N. Dellby, O.L. Krivanek
Nion R&D
Kirkland, WA 98033

Research Division
Almaden - Austin - Beijing - Haifa - India - T. J. Watson - Tokyo - Zurich

Sub-Angstrom Resolution using Aberration Corrected Electron Optics

P.E. Batson

IBM Thomas J. Watson Research Center, Yorktown Heights, New York, 10598, USA

N. Dellby and O.L. Krivanek

Nion R&D, Kirkland, Washington, 98033, USA

Since the invention of electron optics during the 1930's, lens aberrations have limited the achievable spatial resolution to about 50 times the wavelength of the imaging electrons.[1] This situation is similar to that faced by Leeuwenhoek in the 17th century, whose work to improve the quality of glass lenses led directly to his discovery of the ubiquitous "animalicules" in canal water, the first hints of the cellular basis of life. Although the electron optical aberration problem was well understood, more than 60 years elapsed before a practical correction scheme for electron microscopy was demonstrated,[2] and even then the remaining chromatic aberrations still limited the obtained improvement. We report here successful aberration correction in a Scanning Transmission Electron Microscope,[3] which is less sensitive to chromatic aberration, achieving an electron probe smaller than 1 Å for the first time. This performance, about 20 times the electron wavelength at 120 KeV energy, allows dynamic imaging of single atoms, clusters of a few atoms, and single atomic layer "rafts" of atoms coexisting with Au islands on a carbon substrate. Atomic column imaging of semiconductors is now possible using a beam energy which is below the damage threshold for silicon.

Over a half century ago, Scherzer[1] recognized that round electron lenses would suffer from spherical aberration, limiting spatial resolution in an electron microscope to about 2 Å for 100-200 KeV energy electrons. This is unfortunate, because at this resolution the atomic structure of most crystalline materials can be imaged in only one projection. Improving the resolution to 0.5 Å would increase the number of available crystal projections to more than twelve, allowing the 3-dimensional imaging of atomic structure. This problem is illustrated

by the recent detection of individual dopant atoms within bulk semiconductors,[4] where structural characterization of the local environment of the dopant atoms was complicated by the 1.6 Åprobe size, slightly larger than the 1.36 Å distance between atoms in the {110} projection of Si.

Scherzer also pointed out three possible ways to correct the limiting aberrations: i) use of non-round lenses, ii) use of lenses with charge on axis (including mirrors) and iii) use of time-varying fields. Since his work, many attempts have been made to develop practical aberration correctors for the Transmission Electron Microscope, (TEM) culminating in the successful work of Haider and co-workers in the 1990's,[2] which was the first to demonstrate a resolution improvement in a particular instrument. Difficulties remain, however, because the TEM requires a faithful treatment of electron paths which are far from the optic axis, necessitating chromatic aberration correction or addition of an electron monochromator, a task which is not yet complete.

In the late 1960's, an alternative to the TEM imaging geometry was introduced by Crewe and co-workers.[3] They used similar optics to produce a very small electron probe that was scanned in a raster over the area of interest. This geometry, called the Scanning Transmission Electron Microscope (STEM), has become an important tool for quantitative microscopy because many types of analytical signals can be used to produce an image of the scanned area. In particular, Annular Dark Field (ADF) imaging, utilizing high angle elastic scattering which occurs near individual atoms,[5] has emerged as the primary imaging technique. ADF STEM imaging enjoys several advantages over conventional TEM imaging: 1) the spatial resolution is somewhat better; 2) it is sensitive to the atomic number of the imaged atoms; and 3) it provides a positive definite transfer of specimen spatial frequencies, allowing a direct interpretation of results with fewer ambiguities. As the resolution of instruments has improved, ADF imaging has made important contributions to the imaging of individual columns of atoms in crystals[6,7] and, more recently, to the single dopant atom detection within the bulk.[4] Crewe also pointed out the compatibility of the STEM with other analytical techniques, including Electron Energy Loss Spectroscopy (EELS).[8] This technique has proved especially powerful, producing atomic resolution information about atomic species, bonding environment and local electronic structure.[9–11]

The instrument used in this work is based on the VG Microscopes HB501 STEM with the addition of a quadrupole-octupole aberration corrector.[12] Prior to the incorporation of the

corrector, the IBM STEM had been used extensively for ADF imaging and spatially resolved EELS of defects and interfaces in semiconductors.[9] At the 1.9 Å resolution level, it yielded tantalizing, but incomplete information about the atomic structure of important defects such as the dissociated 60° dislocation in Si-Ge/Si structures.[13] The corrector comprises seven major elements: four quadrupoles separated by three octupoles. In addition, minor windings include dipoles and quadrupoles at each stage to allow the control of parasitic aberrations. In all, 35 windings are excited separately using 0.3 ppm stability, computer-controlled current supplies. All axial aberrations up to 5th order in angle are determined by software which analyzes electron shadow images (Ronchigrams[14]) obtained by a TV camera located in the far field behind the specimen. The software then adjusts the corrector to compensate for aberrations up to 4th order. The system spherical aberration (third order) is finally adjusted to about -50 μm to optimally oppose the effects of 5th order aberrations, which are not corrected in the present instrument. Details are described in another publication.[12]

Preliminary imaging of 100 Å Au islands on amorphous carbon have yielded many images similar to that shown in Fig. 1. We see, in addition to the islands, a hierarchy of structures: flat areas with no apparent Au atoms, single atoms, clusters of 2-3 atoms, and 20-50Å wide single layer *rafts* of Au atoms. We identify them as Au layers based in the similarity of their image contrast with that of single atoms produced during dissolution of small Au islands. The monolayer rafts appear to be transition regions between the islands and the more sparsely occupied areas further away, and so it is interesting to speculate that they may play a role in the thermodynamic equilibrium between the islands and the reservoir of atoms elsewhere on the surface.[15] Finally, the single atom contrast was high enough to follow of the motion of atoms under the electron beam: during dissolution of islands and during rapid reformation of islands from dilute groups of atoms.

Fig. 2 summarizes a 10fps acquisition of the interaction between two Au atoms at 300K on the carbon surface. An attractive interaction is clearly visible when the separation is greater than about 1.3-1.5 Å, but at no time do the Au atoms approach closer than this. In this sequence, the two atoms approach, circle one another, separate by about 4 Å and then rejoin. Several things need to be investigated to understand this process: 1) the substrate is clearly complicated, possibly providing low energy channels for atomic motion; 2) the electron beam imparts a finite impulse to the atoms during the imaging process, but the magnitude of this impulse relative to thermal fluctuations needs to be evaluated; 3) higher

speed acquisition may provide information about the diffusion velocity in this situation.

Fourier transform power spectra for the images such as Fig.1 show spatial frequencies as small as 1.17 Å, but this does not give us a good measure of the probe size for several reasons. For instance, small crystal tilts in the islands can lead to blurring of the atom columns. Errors in acquisition of the image intensity, particularly in the low intensity region between atom columns in crystals, can lead to non-physical spatial periodicities.[16] Therefore, we have used images of single Au atoms to evaluate the probe size. This evaluation is summarized in Fig. 3a where we show an image of a single Au atom compared with calculated images for the corrected and uncorrected instrument. We estimate the probe shape based on the measured system aberration parameters, obtained from an analysis of the electron shadow map at the time of the experiment, and the finite source size, obtaining a corrected probe size of 0.74 Å and an uncorrected size of 1.9 Å at 120 KeV. Using a full ADF STEM image calculation for the Au atom,[17] we obtain a corrected image width of 0.75 Å. The visual correspondence is good, but more interestingly, it is obvious that the 1.9 Å resolution is inadequate even to detect single Au atoms in the presence of noise from the carbon support. In Fig. 3b, we compare the 0.75 Å profile with a data obtained from the atom image. Although the statistical quality for the experiment is not sufficient to obtain much detail regarding the shape of the image, certainly the width is consistent with the calculated width.

Fig. 4 shows results for a Ge-Si alloy with and without aberration correction. The shadow maps in Figs. 4a,b. show regions of minimum contrast at the center defining an area constant electron phase, appropriate for use in forming a small probe. The larger available area using aberration correction produces the smaller probe, consistent with the Heisenberg uncertainty relation. Figs. 4c,d. show the resulting crystal image. Markers highlight the well known 1.36 Å "dumbbell" structure formed by the near neighbor atom columns. In Figs. 4e,f. the spatial power spectra for the images are shown. In the uncorrected result, a few spacings out to 1.92 Å are present, illustrating the best previous performance. In the corrected result, many spacings are present, including {551} planes with 0.76 Å spacings. This is a dramatic improvement over that achieved in the past in essentially the same instrument.[12] On a cautionary note, as we mention above, care needs to be applied in interpreting this image because high spatial frequencies can be induced by non-linearities in the image acquisition.[16] This has not been observed in the past at the 1.9 Å resolution, but does appear to be present at some level in the new results. Even so, the dramatic contrasts between the images are

obvious.

To our knowledge, no other electron microscope has ever attained a sub-Å directly interpretable resolution in a single image. Lattice spacings smaller than 1 Å have been observed using high beam energy,[18] and sub-Å resolution has been obtained by *a-posteriori* processing.[19] However, the electron phases in the raw data in such work are always severely distorted, and no structural conclusions are possible without extensive computer processing. Moreover, the acquisition for this approach can exceed one hour, thus exacerbating beam damage, particularly for light elements. Structural resolution much better than 1 Å can also be obtained from electron diffraction data.[20] However, this approach is limited to periodic structures, and also requires extensive computer processing.

The success of aberration correction at this particular time is due to several reasons, many of them linked to recent technical advances: i) computation of electron optical parameters is now possible for non-rotationally symmetric systems, allowing practical designs to be simulated with high accuracy, ii) mechanical fabrication tolerances have advanced materially in the past 15 years, iii) high stability electronic components have become available in the past 10 years, allowing the packaging of many, very high stability, computer controlled, power supplies in a small space, and iv) high speed small computers are now available for real-time processing of the shadow map Rochigram data to obtain aberration parameters.

In conclusion, we believe aberration correction technology combined with the inherent power of the STEM instrument have put us on the threshold of a major step forward in electron optical performance. The new era promises to bring lower voltage, smaller, smarter, more easily managed instruments that will be capable of routinely imaging and analyzing materials at the sub-Å resolution, using several different crystal orientations. Specialized instruments, perhaps using some sub-millimeter sized electrostatic imaging elements, may reach the diffraction limit for the imaging electrons. Multiple corrector systems will allow aberration control of both probe size and detector field of view, in a manner somewhat similar to confocal light microscopy. Finally, detailed control of the amplitude and phase of the incident and scattered electron wavefunction will be possible, allowing specific specimen inelastic transitions to be accessed.[21] In sum, aberration correction truly marks a major shift away from the limited electron optics which have dominated the first 60 years of electron microscopy, and points the way towards a future where precise optical control will allow

routine atomic level characterization of defects and interfaces within the bulk.

---

1. Scherzer, O. The theoretical resolution limit of the electron microscope. *J. Appl. Phys.* **20**, 20 – 29 (1949).
2. Haider, M., Uhlemann, S., Schwan, E., Kabius, B. and Urban, K. Electron microscopy image enhanced. *Nature* **392**, 768 – 769 (1998).
3. Crewe, A.V., Isaacson, M. and Johnson, D. A simple scanning electron microscope. *Rev. Sci. Inst.* **40**, 241–246 (1969).
4. Voyles, P.M., Muller, D.A., Grazul, J.L., Citrin, P.H. and Gossmann, H.-J.L. Atomic-scale imaging of individual dopant atoms and clusters in highly n-doped bulk Si. *Nature* **416**, 826 – 829 (2002).
5. Crewe, A.V., Wall, J. and Langmore, J. Visibility of a single atom. *Science* **168**, 1338 – 1340 (1970).
6. Pennycook, S.J. and Boatner, L.A. Chemically sensitive structure-imaging with a scanning transmission electron microscope. *Nature* **336**, 565–567 (1988).
7. Xu, P., Kirkland, E.J., Silcox, J. and Keyse, R. High resolution imaging of silicon (111) using a 100KeV STEM. *Ultramicroscopy* **32**, 93–102 (1990).
8. Crewe, A.V., Isaacson, M. and Johnson, D. A high resolution electron spectrometer for use in transmission scanning microscopy. *Rev. Sci. Inst.* **42**, 411 – 420 (1971).
9. Batson, P.E. Simultaneous STEM imaging and electron-energy-loss-spectroscopy with atomic-column sensitivity. *Nature* **366**, 727–728 (1993).
10. Muller, D.A., Tzou, Y., Raj, R. and Silcox, J. High resolution EELS at grain boundaries. *Nature* **366**, 725–727 (1993).
11. Browning, N.D., Chisholm, M.F. and Pennycook, S.J. Atomic resolution analysis using a scanning transmission electron microscope. *Nature* **366**, 143–146 (1993).
12. Dellby, N., Krivanek, O.L., Nellist, P.D., Batson, P.E. and Lupini, A.R. Progress in aberration-corrected scanning transmission electron microscopy. *J. Electron Microscopy* **50**, 177 – 185 (2001).
13. Batson, P.E. Structural and electronic characterization of a dissociated 60° dislocation in GeSi. *Phys. Rev. B* **61**, 16633 – 16641 (2000).

14. Ronchi, V. Forty years of history of a grating interferometer. *Applied Optics* **3**, 437 – 450 (1964).

15. Hannon, J.B., Tersoff, J. and Tromp, R.M. Surface stress and thermodynamic nanoscale size selection. *Science* **295**, 299 – 301 (2002).

16. Yu, Z. and Silcox, J. Private communication.

17. Kirkland, E.J. *Advanced computing in electron microscopy.* (Plenum Press, New York, 1998).

18. Kawasaki, T., et al. Development of a 1 MV field emission transmission electron microscope. *J. Electron. Microsc.* **49**, 711 – 718 (2000).

19. O'Keefe, M.A., et al. Sub-Angstrom high resolution transmission electron microscopy at 300 keV. *Ultramicroscopy* **89**, 215–241 (2001).

20. Zuo, J., Y.Kim, O'Keeffe, M. and Spence, J.C.H. Direct observation of d holes and Cu-Cu bonding in Cu_2O. *Nature* **401**, 49 – 56 (1999).

21. Batson, P.E. Symmetry selected electron energy loss scattering in diamond. *Phys. Rev. Lett.* **70**, 1822–1825 (1993).

Figure 1. Atomic resolution image of a Au island on an amorphous carbon substrate. Surrounding the island are "rafts" of single atomic layers of Au. Further away, small clusters and single atoms of Au are present. Diffraction patterns from various regions surrounding the island show that the rafts are ordered in various structures adjacent to the built up islands.

Figure 2. Selected frames from a 10fps acquisition of the interaction of two Au atoms. The interaction is clearly attractive beyond about 1.5 Å and repulsive at smaller distances. Motion occurs in fast jumps, with relatively long periods at rest. At 3.5 sec in this sequence, a jump appears to occur within one frame.

Figure 3. An analysis of the image size of a single Au atom. a)Image of a single Au atom on a carbon support, compared with simulations for the corrected (upper left) and un-corrected (lower left) instrument. The upper left simulation showing a 0.75 Å resolution is a full calculation for the ADF STEM using the Au projected potential, the measured aberration coefficients, and a source size of 0.3 Å, estimated using the source brightness (about 10^9A/cm^2/sterad), the measured probe current (40pA) and the 50mR full illumination angle. The atom would not be visible at the 1.9 Å resolution, shown in the lower left, obtained for C_s= 1.2 mm in the uncorrected instrument. b)Line scan data, obtained from the image, are compared with the 0.75 Å probe calculation.

Figure 4. Summary of results for the {110} projection of $Ge_{70}Si_{30}$. a,b) Ronchigram shadow maps for uncorrected and corrected imaging. Circles indicate the range of angles used for probe formation. c,d) Images of the {110} projection of the crystal obtained using the conditions in a,b). The image on the left is the result of a sum of several 0.5 sec acquisitions, while that on the right is a sum of several sections cut from a single large area image obtained in 0.5 sec, using a beam current of about 40 pA. e,f) The Fourier power spectra for the two examples in c,d). Spatial frequencies are marked.

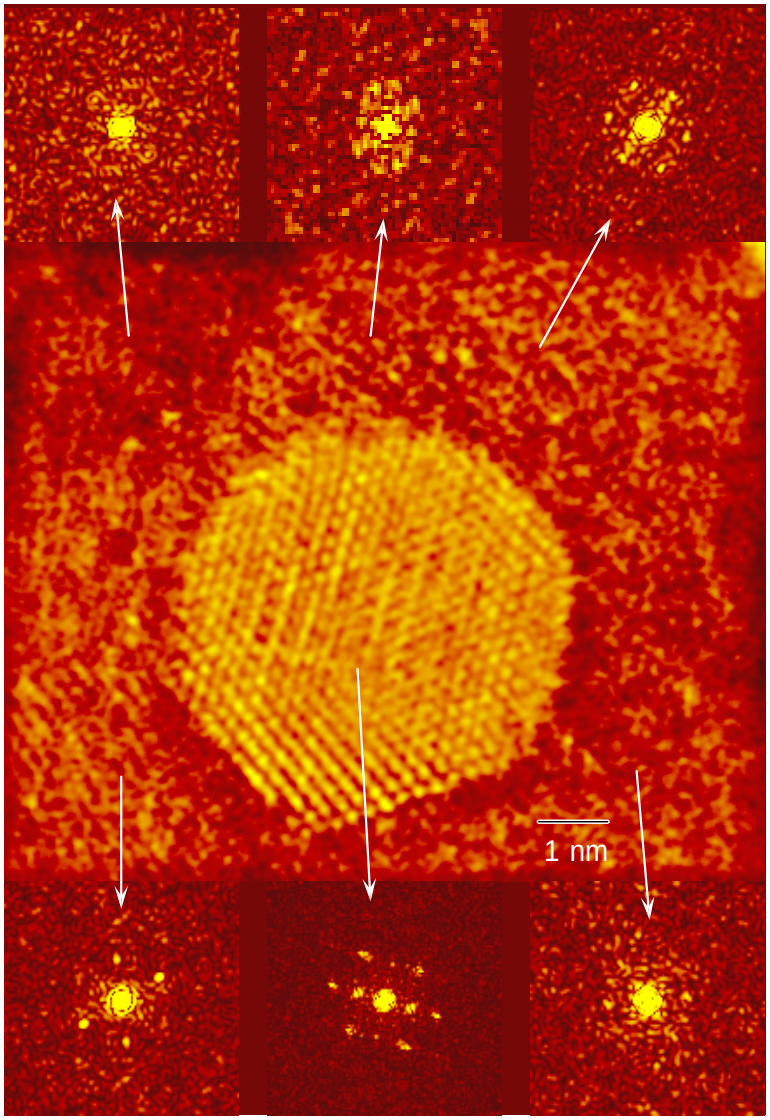

FIG. 1: Batson, et al.

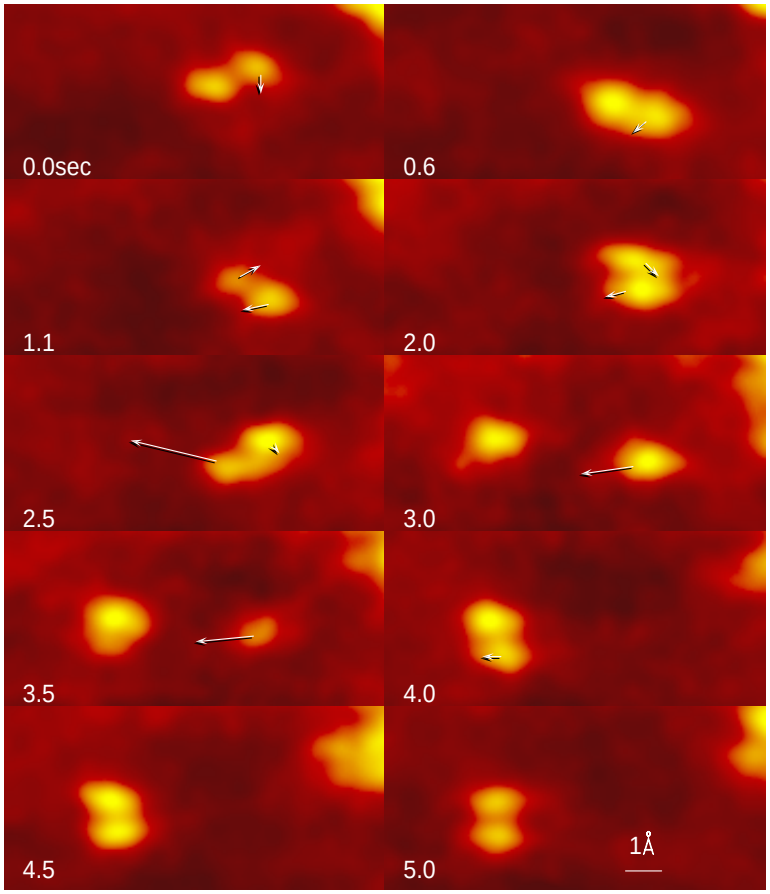

FIG. 2: Batson, et al.

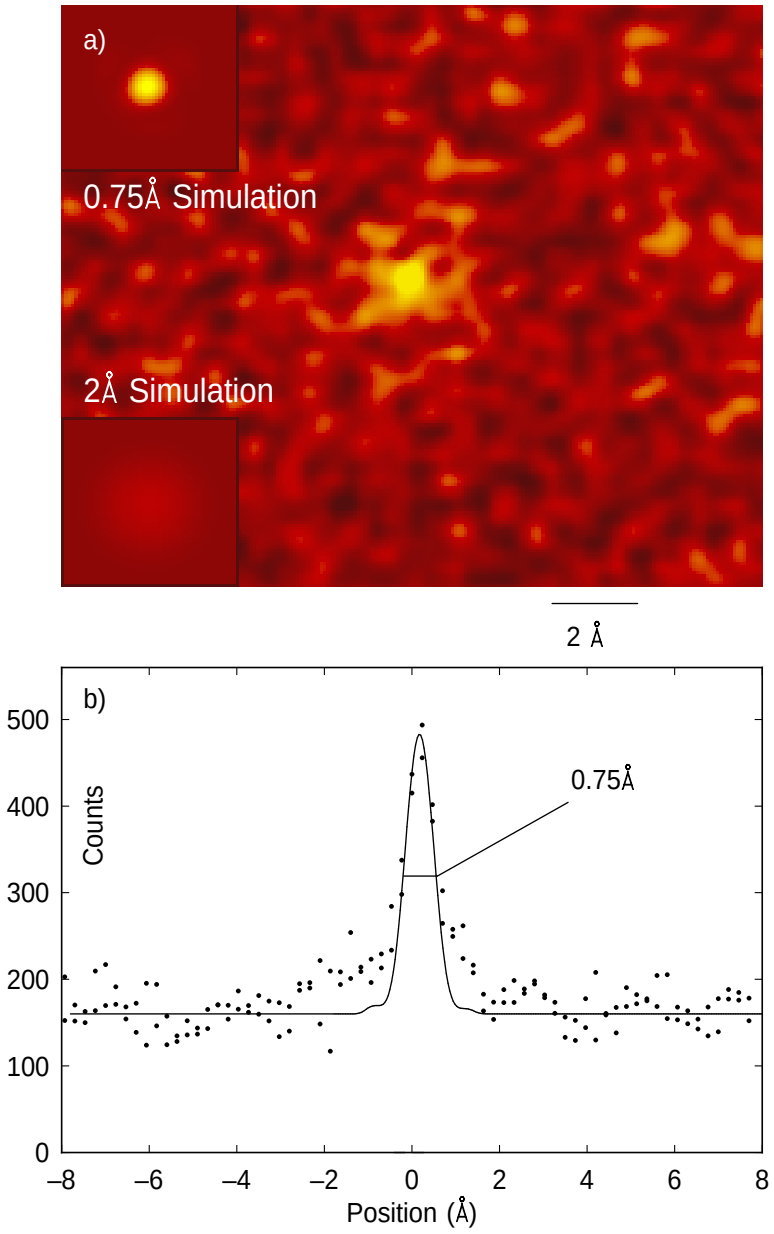

FIG. 3: Batson, et al.

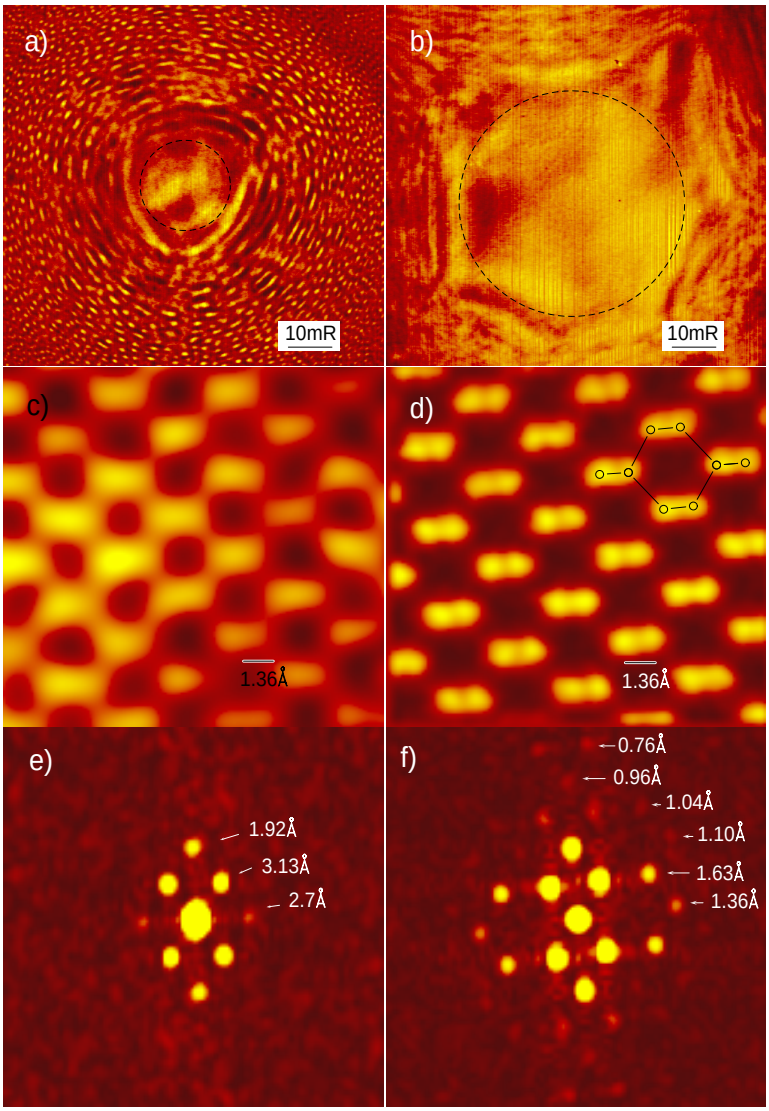

FIG. 4: Batson, et al.